



# HHS Public Access

Author manuscript

*Nat Methods*. Author manuscript; available in PMC 2016 September 28.

Published in final edited form as:

*Nat Methods*. 2016 May ; 13(5): 439–442. doi:10.1038/nmeth.3804.

## Quantitative Super-Resolution Imaging with qPAINT using Transient Binding Analysis

Ralf Jungmann<sup>1,2,5,6</sup>, Maier S Avendaño<sup>1,2,6</sup>, Mingjie Dai<sup>1,3</sup>, Johannes B Woehrstein<sup>1,5</sup>, Sarit S Agasti<sup>1,5</sup>, Zachary Feiger<sup>4</sup>, Avital Rodal<sup>4</sup>, and Peng Yin<sup>1,2</sup>

<sup>1</sup>Wyss Institute for Biologically Inspired Engineering, Harvard University, Boston, Massachusetts, USA

<sup>2</sup>Department of Systems Biology, Harvard Medical School, Boston, Massachusetts, USA

<sup>3</sup>Program in Biophysics, Harvard University, Boston, Massachusetts, USA

<sup>4</sup>Rosenstiel Basic Medical Sciences Research Center, Department of Biology, Brandeis University, Waltham, Massachusetts, USA

### Abstract

Current super-resolution techniques offer unprecedented spatial resolution, but quantitative counting of spatially unresolvable molecules remains challenging. Here, we use the programmable and specific binding of dye-labeled DNA probes to count integer numbers of targets. This method, called quantitative Points Accumulation In Nanoscale Topography (qPAINT), avoids the challenging task of analyzing the environmentally sensitive hard-to-predict photophysics of dyes, and enables robust counting by analyzing the predictable binding kinetics of dye-labeled DNA probes. We benchmarked qPAINT *in vitro* and *in situ* by counting strands on DNA nanostructures, Nup98 protein clusters in the nuclear pore complex, Bruchpilot proteins in *Drosophila*, and finally the number of fluorescence *in situ* hybridization probes on single mRNA targets in fixed cells. We achieved high accuracy (~98–99 %), high precision (~80–95 %), and multiplexed detection over a large dynamic range.

---

Users may view, print, copy, and download text and data-mine the content in such documents, for the purposes of academic research, subject always to the full Conditions of use: [http://www.nature.com/authors/editorial\\_policies/license.html#terms](http://www.nature.com/authors/editorial_policies/license.html#terms)

Correspondence should be addressed to P.Y. ([py@hms.harvard.edu](mailto:py@hms.harvard.edu)).

<sup>5</sup>Present addresses: Max Planck Institute of Biochemistry and Ludwig Maximilian University, Munich, Germany (R.J. and J.B.W.); Jawaharlal Nehru Centre for Advanced Scientific Research (JNCASR), Jakkur, Bangalore, India (S.S.A).

<sup>6</sup>These authors contributed equally to this work.

### AUTHOR CONTRIBUTIONS

R.J. and M.S.A. conceived of the study, designed and performed the experiments, analyzed the data, developed software, and wrote the manuscript. M.D. developed software, and wrote the manuscript. J.B.W. helped with *in vitro* experimental design, and wrote the manuscript. S. S. A. helped with DNA-dye conjugation and developed the antibody labeling protocol. Z.F. and A.R. helped with Brp experiments. P.Y. conceived of and supervised the study, interpreted the data and wrote the manuscript. All authors reviewed and approved the manuscript.

### COMPETING FINANCIAL INTERESTS

The authors declare conflict of interests and have filed a patent application. P.Y. and R.J. are co-founders of Ultivue, Inc., a startup company with interest to commercialize the reported technology.

Note: Supplementary information is available in the online version of the paper.

Optical super-resolution microscopy is revolutionizing the way we study biology. It allows researchers to achieve a spatial resolution below the diffraction-limit of light<sup>1</sup>, providing insights that were previously untraceable<sup>2</sup>. Super-resolution studies often focus on the visualization of synthetic or cellular structures with sub-diffraction spatial resolution. However, datasets obtained by stochastic switching and readout methods<sup>3–5</sup> contain a wealth of information that can be explored for quantitative studies<sup>6–13</sup> beyond “just” binning molecule localizations for spatial visualization. These counting techniques typically rely on complex modeling of blinking properties for target-bound fluorescent dyes. However, current methods face difficulties to accurately and precisely quantify the number of target-bound fluorophores, especially for a large number of fluorescent proteins or dyes in dense clusters. First, the dyes typically have environmentally-sensitive complex photophysics that are hard to model, and different switching properties for dissimilar dyes further complicates multiplexed quantitative imaging<sup>14</sup>. Furthermore, irregular sample illumination or varying excitation and activation intensities can lead to variation in switching kinetics and thus inaccurate quantification<sup>13</sup>. Additionally, target-bound dyes can be bleached pre-maturely before sufficient localizations are collected to allow for accurate and precise quantification.

We introduce a simple and robust quantitative super-resolution method called quantitative PAINT (or qPAINT) based on DNA-PAINT technique<sup>15–19</sup>. Instead of relying on stochastic switching of target-bound dyes<sup>3, 4</sup>, DNA-PAINT achieves apparent blinking of targets via transient binding of free-floating dye-labeled “imager” strands to complementary target-bound “docking” strands. By analyzing the predictable binding kinetics between the imager and docking strands, qPAINT counts the number of targets without spatially resolving them. Compared to existing quantification methods, qPAINT has two unique features: it explicitly decouples blinking from dye photophysics and is immune to photobleaching (as dye-labeled imager strands are continuously replenished from the solution). Thanks to these features, qPAINT represents a conceptual framework that can simultaneously achieve high accuracy, precision, wide dynamic range, robustness, and multiplexing capability for quantifying the number of labeled targets. More specifically, by explicitly avoiding the challenging task of analyzing the hard-to-predict photophysical kinetics of dyes (which may further vary due to non-uniform illumination), qPAINT achieves high quantification accuracy. Immunity to photobleaching permits arbitrarily long imaging time, and hence good statistics and high precision. The easily adjustable influx rate of the imager strands makes such high accuracy and precision achievable over a wide dynamic range. Consistent, predictable, and easily calibratable (when required) binding kinetics allows qPAINT to work robustly under diverse conditions and with different dyes. Finally, by decoupling the apparent blinking from the photophysical properties of dyes, qPAINT is easily multiplexable (spectrally and sequentially<sup>17</sup>).

Fig. 1 illustrates the principle of qPAINT with the example of protein quantification in resolution-limited spots in a fixed cell. The region in Fig. 1a consists of one protein spaced about 200 nm away from a small cluster formed by three proteins (which are spaced ~5 nm apart). Current super-resolution techniques – let alone diffraction-limited imaging – fall short of individually resolving the proteins in the small cluster. Thus, simple spatial counting would under-estimate the total number of proteins. However, by analyzing the predictable and programmable binding kinetics of imager strands in DNA-PAINT rather than spatially

resolving individual targets, it is possible to quantify integer numbers of molecules in these resolution-limited areas. Single-molecule DNA hybridization and dissociation can be described using a simple kinetic model with a second order association rate  $k_{\text{on}}$  and a first order dissociation rate  $k_{\text{off}}$ . These kinetic constants determine the fluorescence on- and off-times ( $\tau_{\text{b}}$  for bright-time and  $\tau_{\text{d}}$  for dark-time, respectively).  $\tau_{\text{b}}$  is linked to  $k_{\text{off}}$  via:  $\tau_{\text{b}} = k_{\text{off}}^{-1}$  and  $\tau_{\text{d}}$  is linked to the influx rate of imager strands  $\xi = k_{\text{on}} \cdot c_{\text{i}}$  by  $\tau_{\text{d}} = (k_{\text{on}} \cdot c_{\text{i}})^{-1} = \xi^{-1}$ , where  $c_{\text{i}}$  is the imager strand concentration. If a single protein molecule labeled with a single docking strand “blinks” with a frequency of 2 in a certain time interval, then three molecules (containing three docking sites) will blink with a three times higher frequency of 6, given a constant influx rate  $\xi$  (Fig. 1a). To practically quantify the number of binding sites from the intensity vs. time traces, we first determine the mean dark-time  $\tau_{\text{d}^*}$  from the cumulative distribution function (Supplementary Fig. 1) in an area of interest, and then calculate the number of binding sites as  $(k_{\text{on}} \cdot c_{\text{i}} \cdot \tau_{\text{d}^*})^{-1} = (\xi \cdot \tau_{\text{d}^*})^{-1}$ .

First, we performed qPAINT *in silico* experiments by stochastically simulating DNA-PAINT data and plotted the results obtained by qPAINT vs. the “true” molecule number used as input (Fig. 1b). Their linear relationship over a wide range of binding sites shows that counting with qPAINT is feasible (see Supplementary Fig. 2 for discussion regarding binding frequency readout). qPAINT’s counting precision ( $1 - c_{\text{v}}$  with  $c_{\text{v}} = \sigma/\mu$ : coefficient of variation with  $\sigma$  and  $\mu$  standard deviation and mean, respectively) can be increased by optimizing the probe influx rate  $\xi$  or extending image acquisition (Supplementary Fig. 3).

Next, we experimentally benchmarked qPAINT *in vitro* and compared it to *in silico* results. We adopted a DNA origami<sup>20</sup>-based imaging quality benchmark platform and accompanying drift-correction and high-resolution image analysis method<sup>21</sup>. The origami was designed to display 12 binding sites that can be visually separated using the advanced image analysis method (Fig. 2a, design details: Supplementary Fig. 4). The visually counted (“ground truth”) number of sites can be compared to the qPAINT analysis for the same structure omitting any *a priori* spatial information (Fig. 2b). High-resolution DNA-PAINT imaging revealed that not all origami showed 12 binding sites (Fig. 2b, see also Supplementary Fig. 5), likely resulting from missing docking strands<sup>15</sup> (see Supplementary Fig. 6 for incorporation efficiency measurement). Comparing qPAINT *in vitro* and *in silico* (Fig. 2c) vs. the ground truth showed good agreement (90 % precision, 97 % accuracy). By adjusting the imager influx rate to  $\xi = 0.03 \text{ s}^{-1}$  and extending image acquisition time, precision and accuracy was improved to 95.4 % and 99.6 %, respectively (Fig. 2c and Supplementary Fig. 7). This now allowed us to distinguish between integer numbers of sites (i.e. between 9, 10, 11, and 12, Fig. 2d). While counting of a few molecules is possible using i.e. stepwise photobleaching approaches<sup>22</sup> or photon statistics<sup>23</sup>, these fail to deliver for higher fluorophore densities<sup>24</sup>. We then showed similar qPAINT performance for such a higher target density: Reanalyzing the dataset but now grouping four DNA origami in one region of interest for qPAINT analysis allowed us to assay qPAINT’s performance for counting 48 sites (Fig. 2e, note that spatial information was still disregarded). Again, qPAINT vs. ground truth analysis showed good agreement (Fig. 2f, 98 % accuracy, 85 % precision). Additionally, we performed qPAINT on DNA origami with 12, 48, and 150 binding sites, respectively, yielding similar performance (see Supplementary Fig. 4 and 8 for design and results). Next, we performed an *in silico* study to determine the counting error for

a given set of binding sites and imager strand influx rate  $\xi$  (Fig. 2g). The results show that  $\xi$  can be tuned to select an optimal “working” point depending on the expected number of binding sites, thus achieving high counting precision over a wide dynamic range. Specifically, one should be able to obtain counting errors below 10 % independent of the number of binding sites. Finally, we demonstrated the ability of qPAINT to count multiple target species in the same sample with similar performance by performing Exchange-PAINT<sup>17</sup> on three distinct DNA origami structures in the same sample (Fig. 2h) using orthogonal imager strand sequences.

Moving from a clean *in vitro* to a more complex *in situ* environment, we next evaluated qPAINT on DNA origami structures bound to cell surface proteins or microinjected in the nuclear and cytoplasmic regions of fixed cells (Supplementary Fig. 9). In both cases, qPAINT performed favorably, achieving similar accuracy and precision as compared to *in vitro* DNA origami results. Comparing nuclear and cytoplasmic counting results yielded similar numbers, demonstrating the consistent binding kinetics of qPAINT in different locations in fixed cells and suggesting its applicability e.g. for counting proteins or DNA or RNA molecules *in situ*.

We next benchmarked qPAINT’s performance *in situ* by quantifying the number of individual units that form the symmetrical ring structure of the Nuclear Pore Complexes (NPCs) by targeting the nucleoporin Nup98 (anchored mainly to the inner ring of the NPC<sup>25, 26</sup>) in U2OS cells using monoclonal primary antibodies directly conjugated to docking strands (Fig. 3a). Due to variation of Nup98-protein-units present in each NPC and potential imperfect antibody labeling (Fig. 3a), not all complexes show the same number of individual proteins units (Fig. 3b and Supplementary Fig. 10). We first used single isolated Nup98 protein clusters as calibration for the probe influx rate and then subsequently grouped NPC structures according to their number of visible Nup98 protein units. We then plotted for each group the distribution obtained by qPAINT vs. the visually determined ground truth and obtained 95 % accuracy and 84 % precision (Fig. 3c).

We then applied qPAINT to quantify the number of single Bruchpilot proteins (Brp), which are structural and functional components of the cytomatrix at the synaptic active zone (CAZ) in the *Drosophila* neuromuscular junction (NMJ)<sup>27</sup>. Here, we used monoclonal primary antibodies (Brp<sup>Nc82</sup>)<sup>12, 27</sup> and DNA-conjugated secondary antibodies for labeling. Similar to a previous study<sup>12</sup>, we defined a CAZ unit as an interconnected region of Brp molecules with an elliptical shape (Fig. 3d, inset **i**, and Supplementary Fig. 11). Subsequent qPAINT yielded  $142 \pm 39$  Brp molecules per CAZ, consistent with previously reported numbers using quantitative dSTORM<sup>12</sup> (Fig. 3e). Note that more than one secondary antibody can be bound per primary antibody. This together with the variability of antibodies bound per subunit will lead to a larger “labeling” variability. However, unlike previous work involving elaborate calibration, qPAINT simply uses single isolated targets to calibrate the influx rate.

Finally, we applied qPAINT to quantify the number of probes bound to an mRNA target (SUZ12) in single-molecule fluorescence *in situ* hybridization (smFISH) experiments (Fig. 3f, see Supplementary Fig. 12 for a larger view of the entire cell). We used a probe set of 64 smFISH probes<sup>28</sup> consisting of a 5’-Cy3b label and a docking strand on the 3’-end (inset

Fig. 3f). After cell fixation, labeling<sup>29</sup> (see Online Methods for details), and imaging, co-localization between Cy3b and DNA-PAINT was observed (Fig. 3f). Subsequent qPAINT analysis yielded – for the first time to our knowledge – the number of *in situ* bound smFISH probes per mRNA molecule. The bimodal distribution showed a first peak at ~45 and a second peak at ~90, consistent with one and two mRNA molecules in a resolution-limited area, respectively (Fig. 3g). Note that counting less than the designed 64 smFISH strands is expected, as likely not all FISH-probes were bound at each mRNA molecule. This experiment thus indicates that ~70 % from all designed smFISH probes were bound to their targets, with a variance of ~36 %.

In conclusion, we described qPAINT, a simple, robust, and precise method to count integer numbers of targets from DNA-PAINT super-resolution datasets, independent of modeling photophysical blinking kinetics of fluorophores. High counting accuracy is achieved by avoiding “undercounting” errors due to already photobleached or “inactive” dye labels and “overcounting” errors due to unaccounted blinking artifacts<sup>10, 30</sup>. Photobleaching is not an issue in qPAINT as dyes are continuously replenished from the solution (see Supplementary Fig. 13), ensuring high counting precision, as a virtually infinite number of “switching” or blinking cycles can be achieved. Importantly, qPAINT works robustly under diverse experimental conditions with consistent high accuracy and precision (e.g. see Fig. 3 and Supplementary Fig. 14 for day-to-day reproducibility).

Although qPAINT achieves consistent and robust counting accuracy and precision for labeled targets, we still face, together with the field of super-resolution microscopy, the challenge to achieve stoichiometric labeling of native protein targets. Imperfect labeling could potentially lead to undercounting. Similar to previous quantitative dSTORM<sup>12</sup>, we opted to use standard immunostaining to label endogenous protein targets with antibodies and obtained comparable quantification results but with a simpler *in situ* calibration using isolated single targets. For future quantification of proteins in compact clusters alternative labeling techniques (e.g. nanobodies<sup>31</sup>, aptamers<sup>32</sup>, modified amino acids<sup>33</sup>, or small molecule binders) need to be developed. In the present work, we demonstrated qPAINT using DNA-PAINT, but the general concept may be generalized to other PAINT methods (e.g. recently developed IRIS probes<sup>34</sup>).

## ONLINE METHODS

### Materials

Non-modified and amino-modified DNA oligonucleotides were purchased from Integrated DNA Technologies (Coralville, IA). Fluorescently-labeled DNA oligonucleotides were purchased from Biosynthesis (Lewisville, TX). Biotinylated monoclonal antibody against EGF receptor was purchased from Cell Signaling (Cat. No. 6627, Danvers, MA). Streptavidin was purchased from Invitrogen (S-888, Carlsbad, CA). Bovine serum albumin (BSA), BSA-Biotin and Triton X-100 was obtained from Sigma Aldrich (A8549, St. Louis, MO). Whole cell blue stain was obtained from Thermo Scientific (8403501, Rockford, IL). Glass slides and coverslips were purchased from VWR (Radnor, PA). Lab-Tek II chambered coverglass were purchased from Thermo Fisher Scientific (Billerica, MA). M13mp18 scaffold was obtained from New England Biolabs (Ipswich, MA). Freeze ‘N Squeeze

columns were ordered from Bio-Rad (Hercules, CA). Paraformaldehyde and glutaraldehyde were obtained from Electron Microscopy Sciences (Hatfield, PA). Protocatechuic acid (PCA), Protocatechuate-3,4-dioxygenase (PCD), and Trolox (TX) were purchased from Sigma Aldrich (37580-25G-F (PCA), P8279-25UN (PCD), 238813-5G (TX)) (St. Louis, MO).

Four buffers were used for sample preparation and imaging: Buffer A (10 mM Tris-HCl, 100 mM NaCl, 0.05 % Tween-20, pH 7.5), buffer B (5 mM Tris-HCl, 10 mM MgCl<sub>2</sub>, 1 mM EDTA, 0.05 % Tween-20, pH 8), buffer B<sup>+</sup> (5 mM Tris-HCl, 10 mM MgCl<sub>2</sub>, 1 mM EDTA, 0.05 % Tween-20, pH 8, supplemented with 1 mM PCA, 1 mM PCD, and 1 mM TX), and buffer C (1×PBS, 500 mM NaCl, pH 8).

### Super-resolution optical setup

Fluorescence imaging was carried out on an inverted Nikon Eclipse Ti microscope (Nikon Instruments, Melville, NY) with the Perfect Focus System, applying an objective-type TIRF configuration using a Nikon TIRF illuminator with an oil-immersion objective (CFI Apo TIRF 100×, NA 1.49, Oil), corresponding to a final pixel size of 160 nm. Three lasers were used for excitation: 488 nm (200 mW nominal, Coherent Sapphire, Santa Clara, CA), 561 nm (200 mW nominal, Coherent Sapphire) and 647 nm (300 mW nominal, MBP Communications, Canada). The laser beam was passed through cleanup filters (ZT488/10, ZET561/10, and ZET640/20, Chroma Technology, Bellows Falls, VT) and coupled into the microscope objective using a multi-band beam splitter (ZT488rdc/ZT561rdc/ZT640rdc, Chroma Technology). Fluorescence light was spectrally filtered with emission filters (ET525/50m, ET600/50m, and ET700/75m, Chroma Technology) and imaged on an EMCCD camera (iXon X3 DU-897, Andor Technologies, North Ireland).

### Confocal setup

Confocal imaging was carried out on a Zeiss Axio Observer with LSM 710 scanning laser confocal system (Zeiss, Thornwood, NY) using the following excitation and emission lines: Whole cell blue stain: 25 mW Argon laser (458/488/514 nm) and 490–560 nm emission filter. Cy3: 20 mW DPSS laser (561 nm) and 563–593 nm emission filter.

### Data analysis

Super-resolution DNA-PAINT images were reconstructed using custom-programmed software written in either LabVIEW<sup>15, 17</sup> or MATLAB<sup>21</sup> for spot-finding and 2D-Gaussian fitting<sup>15, 17</sup>. Drift correction and super-resolution imaging analysis for the 20 nm grid origami sample was performed using custom MATLAB software to visually separate the binding sites<sup>21</sup>. Subsequent qPAINT analysis was performed using a custom-written software implemented in LabVIEW. Both reconstruction and analysis programs are available upon request. After single-molecule reconstruction, the qPAINT analysis software uses a region of interest as input (either automatically or interactively selected) for the binding kinetics analysis. The software determines the mean dark time  $\tau_{d^*}$  by first creating a cumulative distribution function (cdf) from all dark times  $t$  and subsequently fitting this distribution to a single exponential function<sup>15</sup>:

$$P(t)=1-\exp(-t/\tau_{d*}),$$

with  $P$  representing the binding probability for a DNA-PAINT imaging probe at time  $t$  after a previous unbinding event. Finally – after calibrating the imager probe influx rate  $\xi = k_{\text{on}} \cdot c_i$  from a known calibration sample (i.e. previously established from experiments under similar conditions or *in situ* DNA origami calibration standards) – the number of binding sites in the selected region of interest is obtained by

$$\text{binding sites} = \frac{1}{\tau_{d*} \cdot \xi}$$

### qPAINT data simulation

*In silico* qPAINT experiments were performed using COPASI<sup>35</sup>. In brief, a bimolecular chemical reaction model – modeling DNA hybridization and dissociation reactions – with two species (docking and imager strands) and two rate constants (association rate  $k_{\text{on}}$  and dissociation rate  $k_{\text{off}}$ ) was used. Using a direct stochastic solver, we performed time-lapsed simulations that yielded binarized single-molecule intensity vs. time traces. These traces were then subjected to the same qPAINT analysis software that was used to analyze the experimental data (see above). Simulation parameters were selected in accordance to the respective experimental conditions.

**Simulation conditions**—For the simulation in Fig. 1b, two probe influx rates ( $0.005 \text{ s}^{-1}$  and  $0.01 \text{ s}^{-1}$ ) were used, corresponding to 5 nM and 10 nM imager strand concentration at a constant association rate  $k_{\text{on}}$  of  $10^6 \text{ (Ms)}^{-1}$ . Simulations were run for 15,000 “frames” at a sampling interval (or “integration” time) of 0.1 s. 200 simulations per data point were performed (mean and standard deviation are plotted in Fig. 1b). More detailed simulation conditions for simulations accompanying experimental data are given in the following paragraphs.

### DNA origami self-assembly

DNA origami structures displaying 12, 44, 48 and 150 DNA-PAINT docking sites were self-assembled in a one-pot reaction with 50  $\mu\text{l}$  total volume containing 10 nM scaffold strand M13mp18, 100 nM folding staples, 100 nM biotinylated staples, and 1  $\mu\text{M}$  DNA-PAINT docking staple strands in folding buffer (1 $\times$ TE Buffer with 12.5 mM  $\text{MgCl}_2$ ). The solution was annealed using a thermal ramp cooling from 90  $^\circ\text{C}$  to 20  $^\circ\text{C}$  over the course of 1.5 h. After self-assembly, structures were purified by agarose gel electrophoresis (2 % agarose, 0.5 $\times$ TBE, 10 mM  $\text{MgCl}_2$ , 0.5 $\times$ SybrSafe) at 4.5 V/cm for 1.5 h. Gel bands were cut, crushed and filled into a Freeze ‘N Squeeze column and spun for 5 min at  $800 \times g$  at 4  $^\circ\text{C}$ . After this, structures were ready for microscopy sample preparation and image acquisition.

## DNA sequences

20 nm grid structures can be found in Supplementary Table 1. Staple sequences for 12 docking sites origami can be found in Supplementary Table 2. Staple sequences for 48 docking sites origami can be found in Supplementary Table 3. Staple sequences for 150 docking sites origami can be found in Supplementary Table 4. Staple sequences for 20 nm grid structures with fixed Cy3 dyes can be found in Supplementary Table 5. Staple sequences for 44 docking sites origami with fixed Cy3 dyes can be found in Supplementary Table 6. M13mp18 scaffold sequence for DNA origami structures can be found in Supplementary Table 7. Sequences for FISH-PAINT probes can be found in Supplementary Table 8. DNA-PAINT docking and imager sequences and biotin docking sequence can be found in Supplementary Table 9.

## Sample preparation, imaging, and analysis of DNA origami structures

**Sample preparation**—For sample preparation, a piece of coverslip (No. 1.5, 18×18 mm<sup>2</sup>, ~0.17 mm thick) and a glass slide (3×1 inch<sup>2</sup>, 1 mm thick) were sandwiched together by two strips of double-sided tape to form a flow chamber with inner volume of ~20 μl. First, 20 μl of biotin-labeled bovine albumin (1 mg/ml, dissolved in buffer A) was flown into the chamber and incubated for 2 min. The chamber was then washed using 40 μl of buffer A. 20 μl of streptavidin (0.5 mg/ml, dissolved in buffer A) was then flown through the chamber and allowed to bind for 2 min. After washing with 40 μl of buffer A and subsequently with 40 μl of buffer B, 20 μl of biotin labeled DNA structures (~300 pM concentration) in buffer B were finally flown into the chamber and incubated for 5 min. The chamber was washed using 40 μl of buffer B<sup>+</sup> for *in vitro* imaging of 20 nm grid structures and buffer B for all other *in vitro* DNA origami experiments.

**Imaging conditions**—The imaging buffer contained 10 nM (Fig. 2b and e) or 15 nM (Fig. 2c and d) Cy3b-labeled imager strands in buffer B<sup>+</sup>, or 20 nM Atto 655-labeled imager strands in buffer B (Supplementary Fig. 8). Imaging chambers were sealed with epoxy before imaging. Image acquisition was carried out with a CCD readout bandwidth of 3 MHz at 14 bit and 5.1 pre-amp gain. No EM gain was used. Imaging was performed using TIR illumination with an excitation intensity of ~5 mW using the 561 nm laser line (Fig. 2b, c, d, and e) or ~40 mW using the 647 nm laser line (Supplementary Fig. 8). 15,000 frames at 10 Hz frame rate were acquired (Fig. 2b, e, h and Supplementary Fig. 8). 50,000 frames at 5 Hz frame rate were acquired (Fig. 2c green data points).

**Data analysis**—Super-resolution images were reconstructed in either custom LabVIEW or MATLAB software as described above. qPAINT analysis on DNA origami structures was performed interactively by selecting a region of interest that was large enough to fully comprise a single DNA origami (compare gray “ROIs” in Fig. 2b). First, 100 random DNA origami structures displaying the same number of binding sites (i.e. 10 spots) were used to calibrate the probe influx rate  $\xi$ . For the imaging conditions used, a probe influx rate of 0.02 s<sup>-1</sup> was determined (Fig. 2c and f orange data points, and Fig 2h) and 0.03 s<sup>-1</sup> (Fig. 2c green data points). These influx rates were then used to perform qPAINT analysis on all DNA origami structures in the sample. qPAINT analysis for the sample in Supplementary Fig. 8 was performed similarly. Here, the probe influx rate was determined by assuming that the 12



binding site origami structures carry on average 10.5 binding sites (determined by visual counting of similar structures in Fig. 2b). Here, a probe influx rate of  $0.0201 \text{ s}^{-1}$  was determined for the imaging conditions used in this experiment.

**Simulation conditions**—qPAINT simulations for Fig. 2c were performed using 9, 10, 11, or 12 binding sites as model input in combination with association and dissociation rates obtained from the experimental data. qPAINT simulations used in Supplementary Fig. 8 were performed in a similar fashion, here, however, using a normal distribution of binding sites with means determined from the experimental data. Standard deviations of the normal distribution were scaled based on the simulated mean value taking the 12 binding site data from Fig. 2b as input. qPAINT simulations for Fig. 2g were performed similarly to simulations in Fig. 1b. Here, binding sites ranging from 2 to 200 binding sites and probe influx rates ranging from  $0.001 \text{ s}^{-1}$  to  $0.05 \text{ s}^{-1}$  were used to perform 200 stochastic simulations per value pair. After analysis, the coefficient of variation ( $c_v = \sigma/\mu$ ), reflecting the counting error is plotted against the number of binding sites and probe influx rate. As before, 15,000 frames at an “integration time” of 0.1 s are simulated.

### Sample preparation, acquisition, and analysis of artificial receptor clusters on cell surfaces

**Sample preparation**—CHO cells were transiently transfected with the construct encoding a human wild-type EGFR fused with the fluorescent protein mEos (pQCEGFRmEOS; a kind gift from Dr. Jeff Werbin, Harvard Medical School) using Lipofectamine (Invitrogen) according to the manufacturer’s instructions. Briefly, for each transfection reaction, 10  $\mu\text{L}$  Lipofectamine was incubated with 250  $\mu\text{L}$  Opti-MEM for 10 min. Next, 4  $\mu\text{g}$  of EGFR-mEos vector plasmid was added and incubated for 30 min. This mixture was added to cells and incubated overnight. Transfections were carried out when CHO cells were at 90 % confluence. After 24 h, approximately 30 % confluence cells per well were seeded into Lab-Tek II chambers for 24 h before fixation. EGF receptors were immunostained using the following procedure: washing in PBS; fixation in a mixture of 3 % paraformaldehyde and 0.1 % glutaraldehyde in PBS for 10 min; 3-times washing with PBS; reduction with  $\sim 1 \text{ mg/ml}$   $\text{NaBH}_4$  for 7 min; 3-times washing with PBS; permeabilization with 0.25 % (v/v) Triton X-100 in PBS for 10 min; 3-times washing with PBS; blocking with 3 % (w/v) bovine serum albumin for 30 min and staining over night with the biotinylated EGFR monoclonal antibody (diluted to 10  $\mu\text{g/ml}$  in 5 % BSA); 3-times washing with PBS; incubation with 20  $\mu\text{g/ml}$  streptavidin (dissolved in 5 % BSA) for 30 min; 3-times washing with PBS; incubation with  $\sim 0.4 \text{ nM}$  of biotinylated Cy3-labeled DNA origami structures (dissolved in 5 % BSA) for 1 hr; 3-times washing with PBS. Finally, imager strands were added in Buffer C for image acquisition.

**Imaging conditions**—For surface-bound origami in Supplementary Fig. 9, 12 nM Atto 655-labeled imager strands in buffer C were used. The CCD readout bandwidth was set to 5 MHz at 16 bit and 5.1 pre-amp gain with 255 EM gain was used. Imaging was performed using highly inclined (HILO) illumination<sup>36</sup> with an excitation intensity of  $\sim 23 \text{ mW}$  using the 647 nm laser line.

**Data analysis**—Super-resolution images were reconstructed as described above. Here, ROI selection for qPAINT was performed in a semi-automated fashion. In brief, the co-localization between diffraction-limited and DNA-PAINT images was used to select the structures (ROIs) bound to the membrane of the cells. Then, diffraction-limited and super-resolved images were aligned by computing the cross-correlation between them and discarding non-co-localizing molecules. After selection, qPAINT quantification was performed as described above. As before, the probe influx rate was determined by assuming that the 12 binding site origami structures carry on average 10.5 binding sites (determined by visual counting of similar structures in Fig. 2b). Here, a probe influx rate of  $0.02136 \text{ s}^{-1}$  was determined, resulting in an association rate of  $k_{\text{on}} = 1.78 \cdot 10^6 \text{ (Ms)}^{-1}$  under these imaging conditions.

### Sample preparation, acquisition, and analysis of DNA origami microinjected into fixed cells

**Sample preparation**—DNA origami structures with 44 binding sites for DNA-PAINT and fixed Cy3-labeled strands were injected into fixed HeLa cells using a Femtojet (Eppendorf, NY). Multiple injections per cell were performed into nuclear and cytoplasmic regions with the origami sample at  $\sim 1 \text{ nM}$  concentration. The incorporation of the structures inside the cells was confirmed by confocal microscopy (Supplementary Video 1) and by deconvolution of a wide-field image stack using Huygens Professional image processing software (Supplementary Video 2).

**Imaging conditions**—For microinjected DNA origami in Supplementary Fig. 9,  $5 \text{ nM}$  655-labeled imager strands in buffer C were used. The CCD readout bandwidth was set to  $3 \text{ MHz}$  at  $14 \text{ bit}$  and  $5.1 \text{ pre-amp gain}$  with no EM gain was used. Imaging was performed using HILO illumination with an excitation intensity of  $\sim 50 \text{ mW}$  using the  $647 \text{ nm}$  laser line.

**Data analysis**—Super-resolution DNA-PAINT images were reconstructed as described above. For qPAINT analysis, DNA origami structures in the cytoplasm were separated from structures in the nucleus by using the DAPI signal for segmentation (Supplementary Fig. 9). After structure selection, quantification was done as described above in order to determine hybridization kinetics for DNA-PAINT probes in nuclear and cytoplasmic regions. For calculating the number of binding sites, the same association rate determined in experiments on cell surfaces ( $k_{\text{on}} = 1.78 \cdot 10^6 \text{ (Ms)}^{-1}$ ) was used, resulting in a probe influx rate of  $0.0089 \text{ s}^{-1}$ . We used the same apparent association rate as imaging and buffer conditions are the same as in the cell surface experiments.

### Sample preparation, image acquisition, and analysis of qPAINT applied to NPCs

**Sample preparation**—The nucleoporin Nup98 was labeled using a custom DNA-conjugated monoclonal antibody. In brief, first a  $5'$ -thiolated DNA-PAINT docking strand (p1 sequence) was reduced with DTT and purified using NAP5 columns from GE Healthcare (Pittsburgh, PA). In a second step, the monoclonal antibody (#2598, Cell Signaling) was cross-linked with a  $50\times$  excess of a maleimide-PEG-succinimidyl ester crosslinker (746223, Sigma Aldrich). Excess of linker that did not react with antibody was removed using Zeba columns (89883, Life technologies). Third, the antibody-linker was

reacted with the reduced 5'-thiolated DNA-PAINT docking strand at 4°C overnight. Finally, after conjugation, the oligo-labeled antibodies were purified by using 100 kDa Amicon ultra filter (UFC510096, Emdmillipore) from unreacted DNA. The sample was then characterized by mass spectrometry, determining that on average each antibody is coupled with two docking strands.

U2OS cells were cultured in DMEM supplemented with 10% fetal bovine serum. Immunostaining was performed using a standard protocol<sup>37</sup>. Cells were grown overnight on 8-well Lab-Tek Chambered Coverglass. The cells were then rinsed with 2.4% PFA for 20 sec in PBS and extracted with 0.4% Triton X-100 in PBS for 3 min. Next, the cells were fixed for 30 min with 2.4% PFA in PBS, quenched for 5 min with 50 mM NH<sub>4</sub>Cl, then extensively washed with PBS (3x, 10 min each), and blocked with 5% BSA in PBS (blocking buffer) for 1 hour. Subsequently, the cells were incubated overnight at 4°C with the DNA-conjugated monoclonal antibody freshly diluted in the blocking buffer and then incubated with DAPI plus drift markers for 5 min. Then cells were washed once with buffer C prior to imaging and finally, imager strands were added in Buffer C for image acquisition.

**Imaging conditions**—For Fig. 3a, 5 nM Cy3b-labeled imager strands in buffer C were used. The CCD readout bandwidth was set to 3 MHz at 14 bit and 5.1 pre-amp gain with no EM gain. Imaging was performed using HILO illumination with an excitation intensity of ~8 mW using the 561 nm laser line. 15000 frames at 5 Hz frame rate were acquired.

**Data analysis**—Super-resolution DNA-PAINT images were reconstructed as described above. For qPAINT analysis, NPC structures in the nucleus were masked from the signal in the cytoplasm using the DAPI signal. Single Nup98 proteins or complete structures were masked using particle filter and automatic structure selection. Quantification was done as described above in order to determine hybridization kinetics for DNA-PAINT probes. The association rate was determined by using the mean value from the Gaussian fitting of the dark time distribution from the individual protein locations (see arrows in Fig. 2a) to  $k_{on} = 1.75 \cdot 10^6 \text{ (Ms)}^{-1}$ , resulting in a probe influx rate of  $0.00875 \text{ s}^{-1}$ . This value was then used to perform all qPAINT calculations.

Distances between each individual Nup98 protein in a NPC was determined by first calculating the coordinates of the center for each structure using circular Hough transform. Then we project the histograms for the cluster of localization from the center forming a linearized intensity profile with a given number of peaks (3–7 spots, see Supplementary Fig. 10). Distances between spots were calculated by fitting the histograms with minimal number of Gaussians, and calculating the intervals between the peaks. This routine was implemented using custom-written MATLAB software.

### Sample preparation, image acquisition, and analysis of qPAINT for quantifying Brp proteins in CAZ-units

**Sample preparation**—The Brp protein was labeled using a monoclonal antibody Brp<sup>Nc82</sup> (nc82, DSHB). For DNA-PAINT, we used custom secondary anti-mouse goat-DNA-labeled antibodies. The secondary antibody was labeled using the same protocol used for the conjugation of the Nup98 antibody.

*Drosophila* crawling third instar larvae fillets were prepared by dissection in ice-cold HL-3.1 and fixed for 10 min using 4 % paraformaldehyde in HL-3.1. The fillets were then permeabilized with 3 washes of 15 min each in PBT (PBS with 0.05% Triton X-100) followed by a 30 min block in PBT containing 1% normal goat serum and 2% BSA. Preparations were incubated with primary antibodies at 4 °C overnight. After one short and three ~ 20 min washing steps, the fillets were incubated with secondary DNA conjugated antibodies for 2 h followed by another three washing steps. Then fillets were washed once with buffer C prior to imaging and finally, imager strands were added in Buffer C for image acquisition.

**Imaging conditions**—For Fig. 3d, 10 nM Cy3b-labeled imager strands in buffer C were used. The CCD readout bandwidth was set to 3 MHz at 14 bit and 5.1 pre-amp gain with no EM gain. Imaging was performed using HILO illumination with an excitation intensity of ~8 mW using the 561 nm laser line. 15000 frames at 10 Hz frame rate were acquired.

**Data analysis**—Super-resolution DNA-PAINT images were reconstructed as described above. For qPAINT analysis, DNA-PAINT signal from synaptic boutons on neuromuscular junctions (NMJ) were masked using anti horseradish peroxidase (HRP-A488). Single Brp molecules or complete CAZ-units were masked using particle filter and automatic structure selection. Quantification was done as described above in order to determine hybridization kinetics for DNA-PAINT probes. The association rate was determined by using the mean value from the Gaussian fitting of the dark time distribution from the individual Brp molecule locations (see Fig. 3d green circles) resulting in a probe influx rate of 0.0023  $s^{-1}$ . This value was then used to perform all qPAINT calculations on individual CAZ-units. This routine was implemented using custom-written MATLAB software.

### Sample preparation, acquisition, and analysis of smRNA-FISH in fixed cells

**Sample preparation**—SUZ12 mRNAs molecules were tagged in fix HeLa cells using single-stranded oligonucleotides in a FISH-like hybridization scheme. mRNAs were labeled with a unique set of 64 DNA single strand oligonucleotides (Supplementary Table 8). Each probe consists of a unique binding sequence to the mRNA (20 nucleotides length), Cy3b coupled to the 5'-end. The 3'-end carries a single-stranded extension for DNA-PAINT (Fig. 3f). For coupling, the oligonucleotides were ordered with 5' amino modifications from IDT (Coralville, IA). Cy3b was orderd as a succinimidyl ester derivative from GE Healthcare (Pittsburgh, PA). After coupling, the dye-labeled DNA strands were purified by using high pressure liquid chromatography<sup>28</sup>. To perform RNA-FISH, we followed a standard protocol<sup>29</sup>. Cells were fixed with pre-chilled methanol (-20 °C) for 30 minutes. Following fixation, cells were hybridized with the probes at 16 mM each in hybridization buffer consisting of 10 % formamide, 2X SSC, and 10 % dextran sulfate (w/v). Samples were then hybridized overnight in a humidified chamber at 37 °C. Following hybridization, samples were washed twice with wash buffer (2X SSC with 10% formamide) for 30 minutes at 37 °C, and then incubated with DAPI plus drift markers for 5 min. Then cells were washed once with buffer C prior to imaging and finally, imager strands were added in Buffer C for image acquisition.

**Imaging conditions**—For Fig. 3f, 5 nM Atto 655-labeled imager strands in buffer C were used. The CCD readout bandwidth was set to 3MHz at 14 bit and 5.1 pre-amp gain with no EM gain was used. Imaging was performed using HILO illumination with an excitation intensity of ~50 mW using the 647 nm laser line.

**Image analysis**—Super-resolution DNA-PAINT images were reconstructed as described above. Here, Bright field and DAPI images were used to identify individual cells. Diffraction-limited Cy3b and DNA-PAINT images were used to detect RNA transcripts. For image processing, a binary brightfield image was merged with a binary DAPI image. The resulting mask was used to segment the cells. Diffraction-limited spots were detected using a script that operates as follows: First, a median filter followed by a Laplacian filter was applied to each image. Then, a threshold was selected to detect individual spots. This procedure enabled us to identify the total number of diffraction-limited spots within each cell. For quantification of diffraction-limited and super-resolved images, they were aligned by computing the cross-correlation between them. After selection, qPAINT quantification was performed as described above for each individual spot in order to determine the number of probes bound to each individual mRNA. For calculating the number of binding sites, the same association rate determined previously ( $k_{on} = 1.78 \cdot 10^6 \text{ (Ms)}^{-1}$ ) was used, resulting in a probe influx rate of  $0.0089 \text{ s}^{-1}$ . We used the same apparent association rate as imaging and buffer conditions are the same as in the experiments in Supplementary Fig. 9.

### Drift correction

**In vitro imaging**—Drift correction was performed with the custom-written MATLAB software<sup>21</sup>. The positions of all DNA origami structures was tracked throughout the duration of each movie and averaged for use as the drift correction trace. In the 20 nm grid super-resolution image (Fig. 2b), an advanced drift correction algorithm<sup>21</sup> was performed to visually separate the individual grid points.

**In situ imaging**—For cellular imaging, 100 nm gold nanoparticles (Sigma Aldrich; 10 nM in buffer C, added before imaging) were used as drift markers. The gold nanoparticles adsorb non-specifically to the glass bottom of the imaging chambers. Drift correction is performed in a similar fashion as for the *in vitro* imaging (see above). The apparent “movement” of all gold nanoparticles in a field of view is tracked throughout the movie. The obtained trajectories are then averaged and used for global drift correction of the final super-resolution image.

### Supplementary Material

Refer to Web version on PubMed Central for supplementary material.

### Acknowledgments

We thank M. T. Strauss and J. Lara for help with DNA origami design and J. Werbin (Department of Systems Biology, Harvard Medical School) for the donation of CHO cells and fruitful discussions. We also thank A. Raj for providing the smFISH sequences, F. Schueder for initial Brp imaging experiments, and H. Soundararajan and J. Paulson for fruitful discussions. This work is supported by a National Institutes of Health (NIH) Director’s New Innovator Award (1DP2OD007292), an NIH Transformative Research Award (1R01EB018659), an NIH grant (5R21HD072481), an Office of Naval Research (ONR) Young Investigator Program Award (N000141110914),

ONR grants (N000141010827 and N000141310593), a National Science Foundation (NSF) Faculty Early Career Development Award (CCF1054898), an NSF grant (CCF1162459) and a Wyss Institute for Biologically Engineering Faculty Startup Fund to P.Y., and a Pew Scholar Award to A.R.. The BRP antibodies were obtained from the Developmental Studies Hybridoma Bank, created by the NICHD of the NIH. R.J. acknowledges support from the Alexander von Humboldt-Foundation through a Feodor-Lynen Fellowship. M.S.A. and M.D. acknowledge support from HHMI International Student Research Fellowships.

## References

1. Hell SW. *Nature methods*. 2009; 6:24–32. [PubMed: 19116611]
2. Xu K, Zhong G, Zhuang X. *Science*. 2013; 339:452–456. [PubMed: 23239625]
3. Betzig E, et al. *Science*. 2006; 313:1642–1645. [PubMed: 16902090]
4. Rust MJ, Bates M, Zhuang X. *Nature methods*. 2006; 3:793–795. [PubMed: 16896339]
5. Sharonov A, Hochstrasser RM. *Proceedings of the National Academy of Sciences of the United States of America*. 2006; 103:18911–18916. [PubMed: 17142314]
6. Lee SH, Shin JY, Lee A, Bustamante C. *Proceedings of the National Academy of Sciences of the United States of America*. 2012; 109:17436–17441. [PubMed: 23045631]
7. Renz M, Daniels BR, Vamosi G, Arias IM, Lippincott-Schwartz J. *Proceedings of the National Academy of Sciences of the United States of America*. 2012; 109:E2989–2997. [PubMed: 23043115]
8. Endesfelder U, et al. *Biophysical journal*. 2013; 105:172–181. [PubMed: 23823236]
9. Puchner EM, Walter JM, Kasper R, Huang B, Lim WA. *Proceedings of the National Academy of Sciences of the United States of America*. 2013; 110:16015–16020. [PubMed: 24043832]
10. Durisic N, Laparra-Cuervo L, Sandoval-Alvarez A, Borbely JS, Lakadamyali M. *Nature methods*. 2014; 11:156–162. [PubMed: 24390439]
11. Zhao ZW, et al. *Proceedings of the National Academy of Sciences of the United States of America*. 2014; 111:681–686. [PubMed: 24379392]
12. Ehmann N, et al. *Nature communications*. 2014; 5:4650.
13. Nieuwenhuizen RP, et al. *PloS one*. 2015; 10:e0127989. [PubMed: 25992915]
14. Dempsey GT, Vaughan JC, Chen KH, Bates M, Zhuang X. *Nature methods*. 2011; 8:1027–1036. [PubMed: 22056676]
15. Jungmann R, et al. *Nano letters*. 2010; 10:4756–4761. [PubMed: 20957983]
16. Lin C, et al. *Nature chemistry*. 2012; 4:832–839.
17. Jungmann R, et al. *Nature methods*. 2014; 11:313–318. [PubMed: 24487583]
18. Inuma R, et al. *Science*. 2014; 344:65–69. [PubMed: 24625926]
19. Schlichthaerle T, Strauss MT, Schueder F, Woehrstein JB, Jungmann R. *Current opinion in biotechnology*. 2016; 39:41–47. [PubMed: 26773303]
20. Rothmund PW. *Nature*. 2006; 440:297–302. [PubMed: 16541064]
21. Dai M, Jungmann R, Yin P. 2016 submitted.
22. Ulbrich MH, Isacoff EY. *Nature methods*. 2007; 4:319–321. [PubMed: 17369835]
23. Ta H, Kiel A, Wahl M, Hertel DP. *Phys Chem Chem Phys*. 2010; 12:10295–10300. [PubMed: 20603676]
24. Coffman VC, Wu JQ. *Trends in biochemical sciences*. 2012; 37:499–506. [PubMed: 22948030]
25. Hoelz A, Debler EW, Blobel G. *Annual review of biochemistry*. 2011; 80:613–643.
26. Strambio-De-Castillia C, Niepel M, Rout MP. *Nature reviews Molecular cell biology*. 2010; 11:490–501. [PubMed: 20571586]
27. Fouquet W, et al. *J Cell Biol*. 2009; 186:129–145. [PubMed: 19596851]
28. Raj A, van den Bogaard P, Rifkin SA, van Oudenaarden A, Tyagi S. *Nature methods*. 2008; 5:877–879. [PubMed: 18806792]
29. Shaffer SM, Wu MT, Levesque MJ, Raj A. *PloS one*. 2013; 8:e75120. [PubMed: 24066168]
30. Endesfelder U, et al. *Molecules*. 2011; 16:3106–3118. [PubMed: 21490558]

31. Ries J, Kaplan C, Platonova E, Eghlidi H, Ewers H. *Nature methods*. 2012; 9:582–584. [PubMed: 22543348]
32. Opazo F, et al. *Nature methods*. 2012; 9:938–939. [PubMed: 23018995]
33. Milles S, et al. *Journal of the American Chemical Society*. 2012; 134:5187–5195. [PubMed: 22356317]
34. Kiuchi T, Higuchi M, Takamura A, Maruoka M, Watanabe N. *Nature methods*. 2015
35. Hoops S, et al. *Bioinformatics*. 2006; 22:3067–3074. [PubMed: 17032683]
36. Tokunaga M, Imamoto N, Sakata-Sogawa K. *Nature methods*. 2008; 5:159–161. [PubMed: 18176568]
37. Szymborska A, et al. *Science*. 2013; 341:655–658. [PubMed: 23845946]

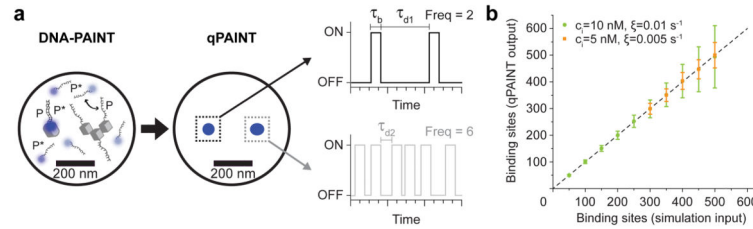


### Figure 1. qPAINT principle

(a) In DNA-PAINT, fluorescently labeled “imager” strands (P\*) transiently bind from solution to complementary “docking” strands (P) attached to a target. Intensity vs. time traces show characteristic fluorescence on- and off-times ( $\tau_b$  and  $\tau_{d1}$ , respectively). qPAINT uses the predictable blinking kinetics to deduct molecule numbers. (b) The number of binding sites can be calculated given a known probe influx rate  $\xi = k_{on} \cdot c_i$ . Stochastic simulations of DNA-PAINT binding events show a linear relationship between simulated and “measured” numbers of binding sites (mean  $\pm$  s.d.). The counting precision for a given number of sites is dependent on the probe influx rate  $\xi$  (green:  $0.01 \text{ s}^{-1}$ , orange:  $0.005 \text{ s}^{-1}$ ).



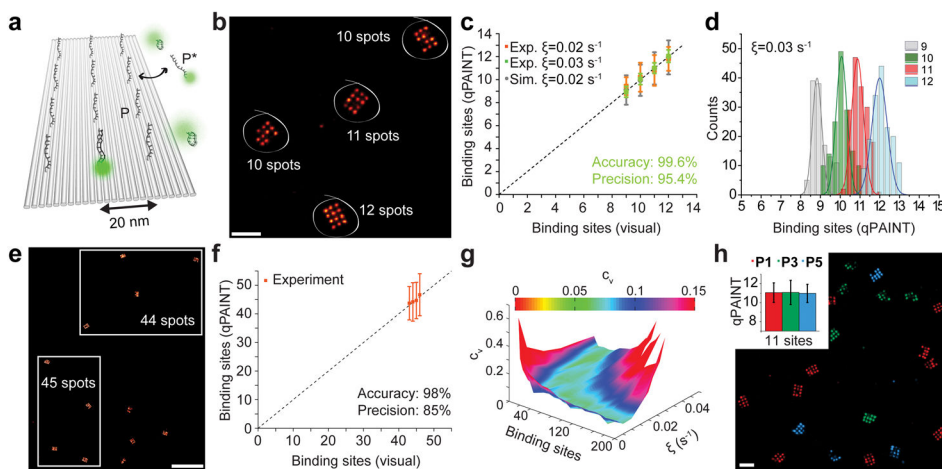


### Figure 2. qPAINT *in vitro* benchmarking

(a) DNA origami structure with 12 designed docking sites. (b) DNA-PAINT image of the structures. (c) Visual counting (x-axis), *in silico* simulation (gray), and *in vitro* experimental qPAINT data (orange and green) are in good agreement (97 % accuracy and 90 % precision for  $\xi = 0.02 \text{ s}^{-1}$  and 25 min imaging time; 99.6 % accuracy and 95.4 % precision for  $\xi = 0.03 \text{ s}^{-1}$  and 166 min imaging time, error bars, 1 s.d.). (d) Distributions plotted from data in c (green data points) demonstrate qPAINT's ability to distinguish between integer numbers of binding sites (i.e. 9 vs. 10 vs. 11 vs. 12; Post Tukey test:  $F(3,605)=1032.52, p<0.01$ , Supplementary Fig. 7). (e) Dynamic range. Same DNA-PAINT dataset as in e (orange data points) reanalyzed by grouping four DNA origami structures together. (f) Comparison between visual counting (x-axis) and *in vitro* (orange) qPAINT analysis shows good agreement (98 % accuracy, 85 % precision, error bars, 1 s.d.). (g) *In silico* analysis of the counting error (coefficient of variation,  $c_v$ ) dependency on the number of binding sites and imager strand influx rate. Tuning  $\xi$  (experimentally adjustable over a wide range) can reach optimal conditions with low counting errors (<10 %) for virtually any number of bindings sites. (h) Multiplexed qPAINT. Three distinct DNA origami structures (similar to c) with orthogonal docking strand sequences (red P1, green P3 and blue P5, error bars, 1 s.d.) were imaged sequentially using Exchange-PAINT. qPAINT analysis on 11 binding sites structures (inset) demonstrates qPAINT's ability to count multiple distinct target species with comparable performance. Scale bars: 100 nm (b and h) and 500 nm (e)

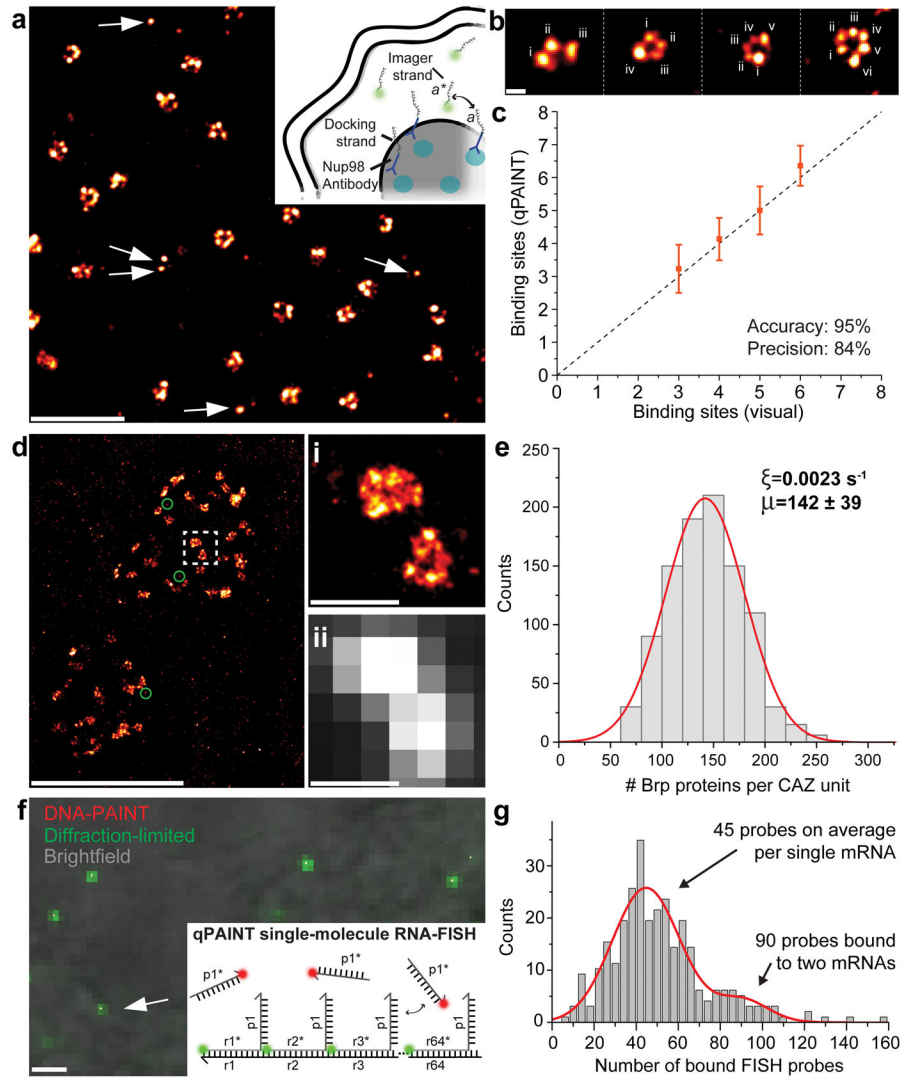


**Figure 3. qPAINT *in situ***

(a–c) qPAINT *in situ* benchmarking with Nup98. (a) DNA-PAINT image of Nup98 proteins in NPCs. Inset: Labeling and imaging schematic for NPC proteins. Single targets (marked with arrows) are used for influx rate calibration. (b) NPC structures displaying three, four, five, and six distinct Nup98 protein clusters were respectively grouped for qPAINT analysis. (c) Comparison between visual counting (x-axis) and qPAINT data (orange) shows good agreement (95 % accuracy and 84 % precision, error bars, 1 s.d.). (d–e) Brp qPAINT experiments. (d) DNA-PAINT image of *Drosophila* NMJs obtained by using secondary DNA-antibody conjugates, and primary monoclonal antibodies against Brp<sup>Nc82</sup>. (i: DNA-PAINT, ii: diffraction-limited) Zoomed-in view of the highlighted area in d showing two separate CAZ-units (assemblies of Brp proteins into multiprotein clusters<sup>12</sup>). (e) qPAINT quantification (n = 981) indicating that the average number of Brp molecules per CAZ-unit is  $142 \pm 39$ . (f–g) smFISH qPAINT experiments. (f) SUZ12 mRNAs molecules are tagged using single-stranded oligonucleotides with binding sequences unique to a part of the target mRNA (r1\* – r64\*), a fixed Cy3b label, and a single-stranded DNA-PAINT docking strand

(p1). (g) qPAINT quantification ( $n = 301$ ) yields ~45 probes bound to a single mRNA molecule (~90 probes for two mRNAs), revealing ~70 % hybridization efficiency of the FISH probes to the mRNA target. Scale bars: 500 nm (**a**, insets **i** and **ii** in **d**), 50 nm (**b**), 1  $\mu\text{m}$  (**d**, **f**)

Author Manuscript

Author Manuscript

Author Manuscript

Author Manuscript